phys. stat. sol. (b) 84, 619 (1977)

Subject classification: 6 and 20.1; 22.7

I. Physikalisches Institut der Rheinisch-Westfälischen Technischen Hochschule Aachen (a) and Physikalisches Institut der Universität Würzburg (b)

A Raman and Far-Infrared Investigation of Phonons in the Rhombohedral V_2–VI_3 Compounds

Bi_2Te_3, Bi_2Se_3, Sb_2Te_3 and $Bi_2(Te_{1-x}Se_x)_3$ $(0 < x < 1)$, $(Bi_{1-y}Sb_y)_2Te_3$ $(0 < y < 1)$

By

W. RICHTER (a), H. KÖHLER (b), and C. R. BECKER (b)

The Raman-active lattice vibrations of Bi_2Se_3, Bi_2Te_3, Sb_2Te_3, and their solid solutions, whose symmetries correspond to the $R\bar{3}m$ space group, are investigated by Raman scattering. Three of the four expected Raman modes, E_g and A_{1g}, could be determined. The FIR optical properties of Bi_2Te_3 crystal surfaces of improved quality ($\boldsymbol{E} \parallel \boldsymbol{c}$ and $\boldsymbol{E} \perp \boldsymbol{c}$) and Bi_2Se_3 ($\boldsymbol{E} \perp \boldsymbol{c}$) are re-examined near helium and room temperature with a Fourier spectrometer, allowing a determination of the infrared-active mode frequencies with higher accuracy. The results for Bi_2Te_3 are compared to the predicted frequencies from the lattice dynamical model, given by Jenkins et al. The frequency shifts of the Raman-active modes in the mixed crystals show single-mode and two-mode behaviour, which is in agreement with simple models for the substitution of antimony and selenium atoms for bismuth and tellurium, respectively, in Bi_2Te_3.

Die Raman-aktiven Gitterschwingungen der Kristalle Bi_2Se_3, Bi_2Te_3, Sb_2Te_3 und ihrer Mischkristallreihen mit der Raumgruppe $R\bar{3}m$ werden durch Raman-Streuung untersucht. Die verschiedenen E_g- und A_{1g}-Raman-Moden können durch Polarisationsmessungen unterschieden werden, wobei drei der vier zu erwartenden Raman-Moden gefunden werden. Die FIR-optischen Eigenschaften von Bi_2Te_3 ($\boldsymbol{E} \parallel \boldsymbol{c}$ und $\boldsymbol{E} \perp \boldsymbol{c}$) und Bi_2Se_3 ($\boldsymbol{E} \perp \boldsymbol{c}$) werden erneut mit Hilfe eines Fourierspektrometers bei Helium- und Raumtemperatur an Kristalloberflächen mit besserer Qualität untersucht, woraus die infrarot-aktiven Eigenfrequenzen mit höherer Genauigkeit bestimmt werden können. Die Eigenfrequenzen für Bi_2Te_3 werden mit den Ergebnissen des gitterdynamischen Modells von Jenkins et al. verglichen. Die Verschiebung der Ramanfrequenzen mit der Mischkristall-Zusammensetzung zeigt Ein-Moden- und Zwei-Moden-Verhalten, die — ausgehend von reinem Bi_2Te_3 — in grober Näherung durch einfache Modelle für die Substitution von Tellur- durch Selen-Atome bzw. Wismut- durch Antimon-Atome erklärt werden können.

1. Introduction

In the last few years the lattice dynamics of Bi_2Te_3 [1 to 3] and the infrared-active lattice vibrations of Bi_2Te_3, Bi_2Se_3, and Sb_2Te_3 [4 to 6] have been studied. The specific heats of Bi_2Te_3 [7] and Bi_2Se_3 [8] were also investigated, yielding the Debye temperatures of these crystals. The thermal conductivity of Bi_2Te_3 [9 to 12] and Bi_2Se_3 [13, 14] was determined as a function of various doping materials and thus the influence of considerable anharmonic effects became apparent. In the Bi_2Te_3–Bi_2Se_3 system the substitution of the tellurium atoms by selenium was investigated by X-ray diffraction yielding the concentration dependence of the lattice constants parallel and perpendicular to the atomic layers [15]. It would be fair to say that most of this work has concentrated on Bi_2Te_3. The data for the elastic constants in the temperature range from 4.2 to 300 K [1] were used to establish a lattice dynamical model with five adjustable parameters [1]. However, the discrepancies between calculated and measured values of the specific heat at low temperatures indicate that the adopted

model, which regards only forces between first and second neighbours, is not sufficient. More distant neighbours and/or the polarizability of the atoms apparently influence the lattice dynamical properties. In order to stimulate improved lattice dynamical calculations the present investigation was undertaken. Raman measurements resulted in the determination of the frequencies of three of the four possible Raman-active phonons. In addition the FIR reflectivity properties were re-examined on crystal surfaces of improved quality. More accurate values for the frequencies and oscillator strengths of the infrared active phonons have thus been obtained.

2. Crystal Structure and Symmetry Properties

All investigated crystals belong to the space group $R\bar{3}m(D_{3d}^5)$, and are composed of hexagonal close-packed atomic layers which are periodically arranged along the c-axis in five layers as follows (see Fig. 1):

$$A_{VI}^{(1)}\text{–}B_V\text{–}A_{VI}^{(2)}\text{–}B_V\text{–}A_{VI}^{(1)}\,.$$

Here the subscript corresponds to the group of the element in the periodic system, and the superscripts on the A atoms designate the different positions within the five-fold layers. A_{VI} may be either Te or Se, and B_V either Bi or Sb. The nearest-neighbour

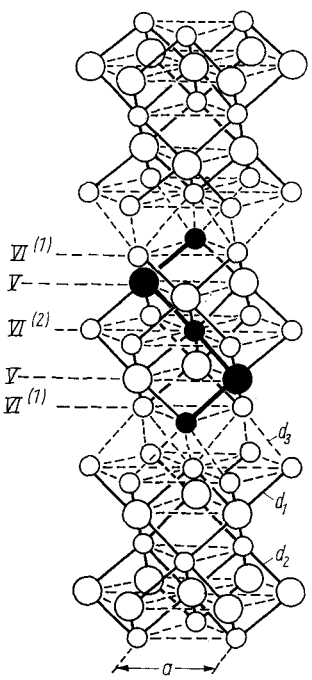

Fig. 1

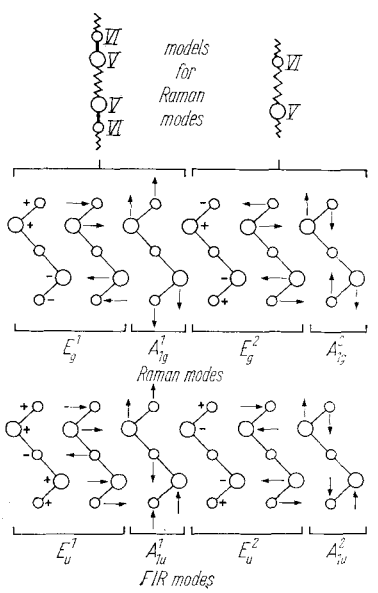

Fig. 2

Fig. 1. Crystal structure ($R\bar{3}m$) of the rhombohedral V_2–VI_3 compounds. Values for d_1, d_2, d_3 are given in Table 1. The solid straight lines correspond to the covalent bonds. The accentuated basis is one of three within a Wigner-Seitz cell of the crystal

Fig. 2. Infrared- and Raman-active modes of the rhombohedral V_2–VI_3 compounds (the superscripts 1, 2 of the E_g, A_{1g}, E_u, and A_{1u} representations correspond to the low- and high-frequency modes, respectively). The linear-chain models for the Raman-active modes as explained in the text, are schematically shown at the top

Table 1
Nearest-neighbour distances (in Å) for atoms in different layers (see Fig. 1) from [16]

	Sb_2Te_3	Bi_2Te_3	Bi_2Se_3
d_1 (V–VI$^{(1)}$)	3.06	3.04	2.99
d_2 (V–VI$^{(2)}$)	3.16	3.24	3.06
d_3 (VI$^{(1)}$–VI$^{(1)}$)	3.64	3.72	3.27

distances between atoms in different monoatomic layers are given in Table 1 for the three pure binary compounds.

Within the fivefold layers covalent bonding is assumed to dominate a small ionic contribution. The valence electron states are thought to form highly excited hybrids of the type sp^3d^2 or p^3d^3 around the B_V lattice sites, which may bind the approximately octahedrally nearest A_{VI} neighbours, three in each of the adjacent $A_{VI}^{(1)}$ and $A_{VI}^{(2)}$ layers. The weaker bonds between the fivefold layers (i.e. between the $A_{VI}^{(1)}$ double atomic layers) are assumed to be of the van der Waals type.

The crystal structure has the following symmetry elements: one trigonal axis perpendicular to the atomic layers, three binary axes parallel to the atomic layers, three mirror planes which contain the trigonal axis and are each perpendicular to one of the binary axis, and finally the $A_{VI}^{(2)}$ atoms are centres of inversion. The primitive unit cell of Bi_2Se_3, Bi_2Te_3, and Sb_2Te_3 contains five atoms in accordance with the chemical formula. There are consequently 15 lattice dynamical modes at $q = 0$, three of which are acoustic modes and 12 optical modes.

Group theory classifies these 12 optical modes into $2A_{1g}$, $2E_g$, $2A_{1u}$, and $2E_u$. The corresponding atomic dispalcements are shown in Fig. 2 for the basis of atoms selected in Fig. 1. Because of inversion symmetry these modes are exclusively Raman- or infrared-active according to the selection rules given in Table 2. It follows that the E_g and A_{1g} modes may be distinguished from one another as a result of the off-diagonal Raman tensor components of the E_g modes. Similarly the symmetry of the infrared-active modes may be ascertained by polarizing the incident light either parallelly (A_{1u}) or perpendicularly (E_u) to the c-axis.

Table 2
Selection rules for one-phonon infrared absorption (IR) and Raman scattering in V_2–VI_3 compounds having R3m symmetry

modes		selection rules	
symmetry	number	Raman	IR
A_{1g}	2	$\begin{pmatrix} a & 0 & 0 \\ 0 & a & 0 \\ 0 & 0 & b \end{pmatrix}$	—
E_g	2	$\begin{pmatrix} c & 0 & 0 \\ 0 & -c & d \\ 0 & d & 0 \end{pmatrix}$ $\begin{pmatrix} 0 & -c & -d \\ -c & 0 & 0 \\ -d & 0 & 0 \end{pmatrix}$	—
A_{1u}	2	—	$\boldsymbol{E} \parallel \boldsymbol{c}$
E_u	2	—	$\boldsymbol{E} \perp \boldsymbol{c}$

The frequencies of the Raman-active modes are discussed here by means of a simple model. To begin with we have assumed that the normal modes are the same as the symmetry modes shown in Fig. 2, i.e. no appreciable mixing of modes with the same symmetry occurs. In the E_g^1 and A_{1g}^1 modes the outer V–VI$^{(1)}$ pairs move in phase (see Fig. 2). Thus the V–VI$^{(2)}$ bonding forces will be primarily involved in these vibrations. The linear-chain approximation with two equal masses $M = m_V + m_{VI}$ per unit cell can then be used for the E_g^1 and A_{1g}^1 modes. From the nearest-neighbour distances (Table 1) and also from the lattice dynamical model used by Jenkins et al. [1] it is reasonable to assume that the nearest-neighbour force constants between V and VI$^{(2)}$ atoms are smaller than those between V and VI$^{(1)}$ atoms. Consequently, one expects the A_{1g}^1 and E_g^1 modes to occur at lower frequencies than the A_{1g}^2 and E_g^2 modes. The latter modes, where the outer V and VI$^{(1)}$ atoms move in opposite phase, will mainly be affected by forces between V and VI$^{(1)}$ atoms. This is represented in this rather crude model as two atoms with masses m_V and m_{VI} in the unit cell (see Fig. 2). This model, though oversimplified, reproduces characteristic features of the experimental results as will be discussed later.

3. Experimental

All crystals were grown in fused silica ampoules by means of a vertical Bridgman technique, starting from 5 N material of the constituents. The crystal bars were sawed by an acid-string saw, using the so-called Honeywell etch (100 g CrO_3; 266 g H_2O; 132 g HCl (32%)). All Raman measurements were performed on cleavage planes perpendicular to the trigonal axis, but the FIR reflectivity had to be measured on polished surfaces containing the c-axis as well as on cleavage planes.

For the Raman scattering experiments both the 5145 Å line of an Ar^+laser and the 6471 Å line of a Kr^+laser were used for excitation. The backscattered light was analysed by a triple monochromator and a photon counting system. The FIR optical reflectivity at nearly normal incidence was investigated with an FIR Polytec Fourier spectrometer. A wire grid on a polyethylene substrate was used to polarize the incident light. Bi_2Te_3 surfaces of good optical quality could be prepared for both $\boldsymbol{E} \perp \boldsymbol{c}$ and $\boldsymbol{E} \parallel \boldsymbol{c}$ polarization conditions, but for Bi_2Se_3 only $\boldsymbol{E} \perp \boldsymbol{c}$ polarization conditions on cleavage planes were possible. This was true because all of the attempted polishing techniques did not yield surfaces of sufficiently high optical quality for the investigations with $\boldsymbol{E} \parallel \boldsymbol{c}$ polarization conditions. The reflectivity data at both room temperature and 15 K were taken with the sample mounted in a cryostat, i.e. nearly identical filtering conditions.

4. Results

4.1 Raman scattering

A typical Raman spectrum for the binary compounds, i.e. Bi_2Se_3, is shown in Fig. 3. The upper curve is the xx component of the Raman tensor, and the lower curve the xy component. Althogether three peaks are observed and one of them was present for xx as well as xy polarization conditions. From the selection rules in Table 2 it follows that this peak has to be assigned to the E_g mode whereas the other two correspond to A_{1g} modes. Since $2E_g$ and $2A_{1g}$ modes are predicted from group theory one of the E_g modes is missing. This was also the case for Bi_2Te_3 and Sb_2Te_3. The observed frequencies are given in Tables 3 and 4. The mixed crystal Raman spectra are shown in Fig. 4a and Fig. 5a for different compositions. The solid line represents A_{1g} symmetry scattering, and the dashed lines represent scattering with E_g symmetry. These phonon frequencies are reproduced in Fig. 4b and Fig. 5b as a function of composition. While there is a continuous variation of frequencies with composition in the Bi_2Te_3–

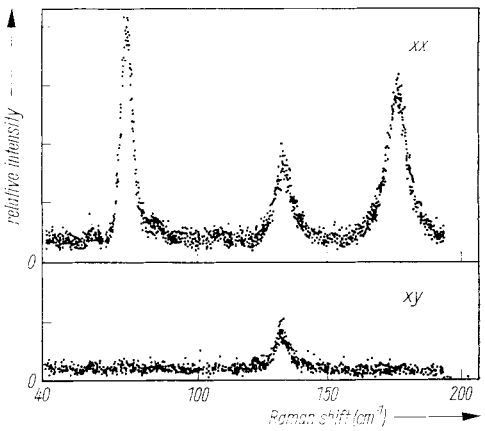

Fig. 3. A typical Raman spectrum of a V_2–VI_3 compound (pure Bi_2Se_3). The upper trace is the xx Raman tensor component and the lower trace is the xy Raman tensor component

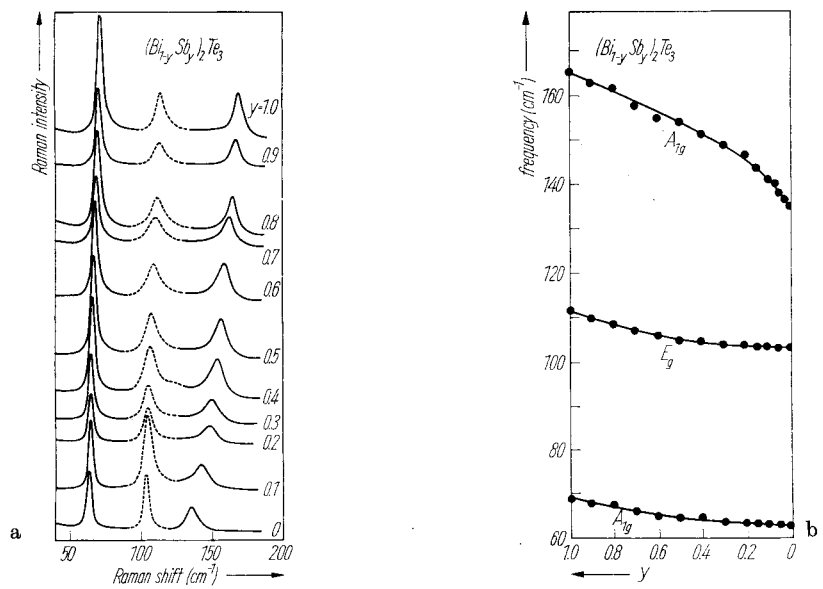

Fig. 4. Experimental data for $(Bi_{1-y}Sb_y)_2Te_3$ mixed crystals ($0 \leqq y \leqq 1$). a) Raman spectra (on the ordinate zero points shifted); b) phonon frequencies plotted versus the composition parameter y

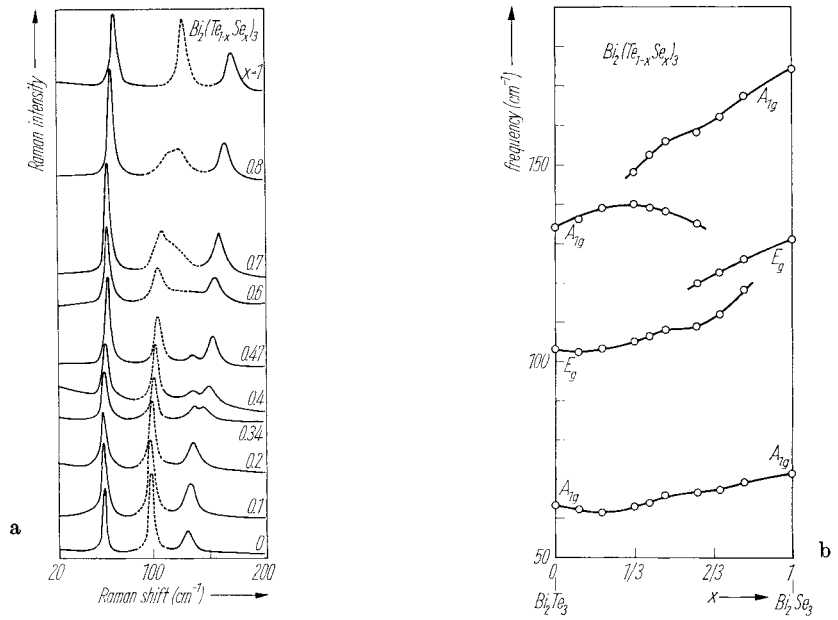

Fig. 5. Raman spectra and corresponding phonon frequencies for $Bi_2(Te_{1-x}Se_x)_3$ ($0 \leqq x \leqq 1$). a) Raman spectra (on the ordinate zero points shifted); b) phonon frequencies versus composition

Sb_2Te_3 system, discontinuities occur in the Bi_2Te_3–Bi_2Se_3 system for intermediate values of the mixing parameter x.

4.2 Infrared reflectivity

The reflectivity curves for Bi_2Te_3 and Bi_2Se_3 at 15 K are shown in Fig. 6a, b and Fig. 7, respectively. The phonon-induced structure in the reflectivity superimposed on the free-carrier contribution is much more pronounced than thas been found in previous measurements [4, 5]. Hence more accurate values of the optical constants could be obtained by a Kramers-Kronig analysis of the reflectivity spectra. Similarly as in [4, 5] a classical oscillator fit resulted in more accurate parameters for the infrared-active phonons which are listed in Tables 3 and 5. These values are quite different from those quoted in [4, 5]. Due to the reasons given above these values are believed to be more accurate. In addition to large values for the oscillator strengths $\Delta\varepsilon$, especially for $\boldsymbol{E} \perp \boldsymbol{c}$, the temperature dependence of the eigenfrequencies is worth noting. In contrast to the usual behaviour they decrease with decreasing temperature. This might be explained along similar lines as the decreasing phonon frequencies found in some hydrostatic pressure experiments [20]. The main effect of the decreasing temperature (equivalent to increasing pressure if one considers only volume effects) in crystals with

Table 3

Comparison of experimental and calculated phonon frequencies for Bi_2Te_3 [1]

mode	frequencies (cm^{-1})	
	observed	calc. [1]
A	134	128.3
	62.5	71.1
E_g	103	118.5
	—	50.6
A_{1u}	120	141
	94	93.5
E_u	95	116.4
	50	84.6

Table 4
Calculated and experimental Raman frequencies (cm^{-1}) for Bi_2Se_3 and Sb_2Te_3

mode	Bi_2Se_3			Sb_2Te_3		
	$\tilde{\nu}_{exp}$	$\tilde{\nu}_{calc}$	$\tilde{\nu}_{exp}/\tilde{\nu}_{calc}$	$\tilde{\nu}_{exp}$	$\tilde{\nu}_{calc}$	$\tilde{\nu}_{exp}/\tilde{\nu}_{calc}$
A_{1g}	174.5	157.5	1.108	165	151	1.093
E_g	131.5	121	1.087	112	116	0.966
A_{1g}	72	67.5	1.067	69	72.5	0.952
E_g	—	—	—	—	—	—

anisotropic bonding properties is to increase the weak force constant by a large percentage, leading to a weakening of the strong bonds. As a consequence, phonon frequencies which are mainly determined by the latter will decrease.

5. Discussion

5.1 Bi_2Te_3

As a result of these and previous measurements the frequencies of seven of the eight expected phonons are known and it should be interesting to compare these values with those calculated by Jenkins et al. [1] with their force constant model, where the measured elastic constants were used as fit parameters. This comparison is made in Table 3. Although the agreement for the Raman-active mode is reasonable, there are large discrepancies for the IR active modes, especially for the low-frequency E_u mode which also has an abnormally large contribution to the dielectric constant $\Delta\varepsilon = 205$. This clearly indicates that short-range central forces alone are insufficient in describing the lattice dynamics of these highly polarizable materials regarded. Estimating the decrease in frequency from the equation $\tilde{\nu}_{TO}^2 = \tilde{\nu}_0^2\,(\varepsilon(\infty)+2)/(\varepsilon(0)+2)$, given by Szigeti [21] for ionic crystals, we obtain a reduction from $\nu_0(E_u) = 84.6\ cm^{-1}$ to $\tilde{\nu}_{TO}(E_u) = 46\ cm^{-1}$ in good agreement with experiment. This shows that long-range Coulomb forces have to be included in a lattice dynamical model for these materials.

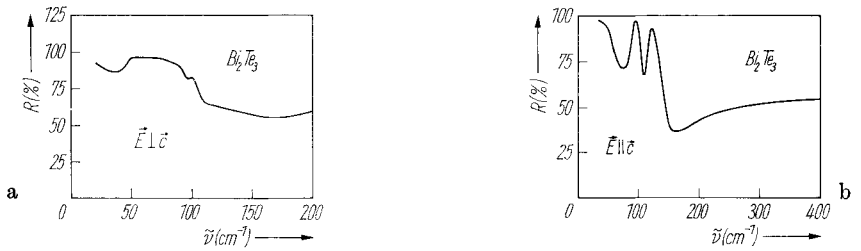

Fig. 6. Infrared reflectivity spectra for Bi_2Te_3 at 15 K: a) $\boldsymbol{E} \perp \boldsymbol{c}$; b) $\boldsymbol{E} \parallel \boldsymbol{c}$

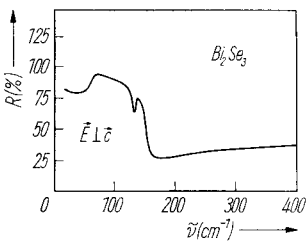

Fig. 7. Infrared reflectivity spectrum for Bi_2Se_3 at 15 K with $\boldsymbol{E} \perp \boldsymbol{c}$

The Raman frequencies for the two other compounds, Bi_2Se_3 and Sb_2Te_3, are compared in Table 4 with values calculated for the corresponding modes of Bi_2Te_3 with the simple models schematically shown in Fig. 2, where in addition it was assumed that the force constants in all three materials are equal (indicated by similar atomic distances, see Table 1). This implies that the frequency shifts originate from the different reduced masses only. These are given by $M_2 = (m_{VI}^{-1} + m_V^{-1})^{-1}$ for the E_g^2 and A_{1g}^2 modes and by $M_1 = 2(m_{VI} + m_V)$ for the low-frequency, E_g^1 and A_{1g}^1 modes.

Regarding Table 4, where the maximum discrepancy is 10%, the assumption of nearly equal force constants seems to be fulfilled quite well. However, for Bi_2Se_3, where all the calculated frequencies are lower than the experimental data, one should assume somewhat stronger bonding forces compared to Bi_2Te_3 and Sb_2Te_3. This fact is also supported by smaller atomic distances in Bi_2Se_3 as listed in Table 1.

5.2 Mixed crystals

The interesting fact to be noted in Fig. 4 and 5 is that in the Bi–Sb–Te system a continuous shift of phonon frequencies between the frequencies of the pure binary compounds occurs, while in the Bi–Te–Se system discontinuities are observed for the two high-frequency modes at intermediate compositions. The former is usually termed one-mode behaviour, the latter two-mode behaviour.

A very small frequency shift of all the Raman modes in the Bi_2Te_3–Bi_2Se_3 system is observed for $0 \leqq x \leqq 1/3$, corresponding to the substitution of less than 1/3 of the tellurium atoms by selenium in Bi_2Te_3. Because two different kinds of the tellurium atoms, $A_{VI}^{(1)}$ and $A_{VI}^{(2)}$, are present and the latter do not participate in the Raman-active vibrations, this suggests that the $Te^{(2)}$ atoms are preferentially replaced by $Se^{(2)}$ atoms up to $x = 1/3$.

Table 5

Experimental infrared-active frequencies and oscillator parameters, which were deduced from a classical oscillator fit. The $\Delta\varepsilon_i$ are the contributions to the dielectric constant and $2\Delta\tilde{\nu}_i$ are the oscillator half-widths

		Bi_2Te_3		Bi_2Se_3		Sb_2Te_3 [6]
		300 K	15 K	300 K	15 K	300 K
$E \perp c$	$\varepsilon(\infty)$	85	85 [17]	29	29 [19]	51
	$\tilde{\nu}_1$ (cm^{-1})	50 ± 2	48 ± 2	65 ± 2	61 ± 2	67
	$2\Delta\tilde{\nu}_1$ (cm^{-1})	10	4	12	10	10
	$\Delta\varepsilon_1$		205		83	500
	$\tilde{\nu}_2$ (cm^{-1})	95 ± 5	98 ± 3	129 ± 5	134 ± 5	
	$2\Delta\tilde{\nu}_2$ (cm^{-1})	15	7	15	8	
	$\Delta\varepsilon_2$		1.5		0.5	
	$\varepsilon(0)$		290		113	≈ 600
$E \parallel c$	$\varepsilon(\infty)$	50	50 [18]			
	$\tilde{\nu}_1$ (cm^{-1})	94 ± 4	88 ± 2			
	$2\Delta\tilde{\nu}_1$ (cm^{-1})	7	6			
	$\Delta\varepsilon_1$		19.5			
	$\tilde{\nu}_1$ (cm^{-1})	120 ± 5	114 ± 2			
	$2\Delta\tilde{\nu}_2$ (cm^{-1})	10	6			
	$\Delta\varepsilon_2$		5.9			
	$\varepsilon(0)$		75			

This conclusion was also drawn from X-ray diffraction measurements in order to describe the variation of the lattice constants in the Bi_2Te_3–Bi_2Se_3 system with composition [15]. For $0 < x < 1/3$ a linear decrease in c (lattice constant in the direction of the trigonal axis) was observed, while for $1/3 < x < 1$ a positive deviation from Vegard's linear law was present. The low-frequency shifts for $0 < x < 1/3$ indicate in addition that, as concluded before, the bonding forces between the Bi and $Te^{(2)}$ atoms are approximately the same as for Bi and $Se^{(2)}$. This is especially evident from the nearly constant frequency of the low-frequency A_{1g} mode in the range $0 < x < 1/3$.

For $x > 1/3$ the $Te^{(1)}$ atoms are primarily replaced by selenium, giving rise to considerable frequency shifts, since in this range the reduced masses vary with x. Although the low A_{1g} frequency shows the one-mode behaviour, two-mode behaviour is exhibited by the high-frequency A_{1g} and E_g modes. Considerable splitting occurs for the A_{1g} branches in particular. The presence of two-mode behaviour indicates that the high-frequency modes are out-of-phase movements of the outer Bi and $Te^{(1)}/Se^{(1)}$ atoms which are attracted by the strongest bonding forces in the crystals [1]. They are almost decoupled from each other, thus allowing different mode frequencies for the Bi–$Te^{(1)}$ and Bi–$Se^{(1)}$ vibrations.

According to the same arguments local modes should be possible in the Sb_2Te_3–Bi_2Te_3 system for compositions close to the pure binary compounds. These frequencies would correspond to Sb–$Te^{(1)}$ or Bi–$Te^{(1)}$ vibrations. However, no experimental evidence for such local modes has been found as can be seen from Fig. 4a.

6. Conclusions

All Raman and infrared phonon frequencies of Bi_2Te_3 were determined except for one of the low-frequency E_g mode. Only five out of eight were observed in Bi_2Se_3 and only four in Sb_2Te_3. A comparison with the predicted $q = 0$ frequencies from the Born-von Kármán lattice model of Jenkins et al. [1] shows some agreement with the Raman-active modes in Bi_2Te_3, however, it shows large discrepancies for the infrared-active modes. In particular the low-frequency mode with its largest oscillator strength ($\Delta\varepsilon = 205$) was predicted to be 60% too high. It is apparently necessary to introduce polarization effects into the lattice dynamical calculations, especially in order to describe the movements of the $Te^{(2)}$ atoms for $\boldsymbol{E} \perp \boldsymbol{c}$. Such calculations should be facilitated by the fact that data on the other homologous compounds are available. In addition it should be noted that inelastic neutron scattering [22] and phonon-assisted tunneling [23, 24] experiments have been performed on Bi_2Te_3 and Sb_2Te_3 recently.

Acknowledgements

We are indebted to the Max-Planck-Institut für Festkörperforschung Stuttgart, where most of the Raman scattering experiments have been performed and to the Deutsche Forschungsgemeinschaft for providing the Polytec FIR 30 Fourier Spectrometer.

References

[1] J. O. Jenkins, J. A. Rayne, and R. W. Ure, Phys. Rev. B **5**, 3171 (1972).
[2] J. Blitz, D. M. Clunie, and C. A. Hogarth, Proc. V. Internat. Conf. Phys. Semicond., Prague 1960, Publ. Czech. Acad. Sci., Prague 1961 (p. 641).
[3] J. Blitz, Brit. J. Non-dest. Test **2**, 2 (1960).
[4] K. H. Unkelbach, C. R. Becker, H. Köhler, and A. von Middendorf, phys. stat. sol. (b) **60**, K41 (1973).
[5] H. Köhler, and C. R. Becker, phys. stat. sol. (b) **61**, 533 (1974).
[6] K. H. Unkelbach, Dissertation, Aachen 1973.

[7] E. S. ITSKEVICH, Soviet Phys. — J. exper. theor. Phys. **11**, 255 (1960).
[8] G. E. SHOEMAKE, J. A. RAYNE, and R. W. URE, Phys. Rev. **185**, 1046 (1969).
[9] C. B. SATTERTHWAITE and R. W. URE, Phys. Rev. **108**, 1164 (1957).
[10] H. J. GOLDSMID, Proc. Phys. Soc. **B69**, 203 (1956); **72**, 17 (1958).
[11] P. A. WALKER, Proc. Phys. Soc. **76**, 113 (1960).
[12] A. E. BOWLEY, R. DELVED, and H. J. GOLDSMID, Proc. Phys. Soc. **72**, 401 (1958).
[13] T. J. GRAY, New York Univ. Coll. Ceram., Semicond. Mater., Semi-Annual Rep. 1960, Contract No. Nonr.-150301, Proj. 015-215 ASTIA AD 244-415.
[14] M. H. LA CHANCE and E. E. GARDNER, Adv. Energy Conversion **1**, 133 (1961).
[15] G. R. MILLER, CHE-YU LI, and C. W. SPENCER, J. appl. Phys. **34**, 1398 (1963).
[16] N. K. ABRIKOSOV, V. F. BANKINA, L. V. PORETSKAYA, L. E. SHELIMOVA, and E. V. SKUDNOVA, in: Semiconductor Phys., Vol. 3 (Semiconducting II–VI, IV–VI and V–VI Compounds), Plenum Press, New York 1969 (p. 164).
[17] I. G. AUSTIN, Procl Phys. Soc. **72**, 545 (1958); **76**, 169 (1960).
[18] R. GROTH and P. SCHNABEL, J. Phys. Chem. Solids **25**, 1261 (1964).
[19] H. GOBRECHT, S. SEECK, and T. KLOSE, Z. Phys. **190**, 427 (1966).
[20] W. RICHTER, J. B. RENUCCI, and M. CARDONA, phys. stat. sol. (b) **56**, 223 (1973).
[21] B. SZIGETI, Dielectric Theory of Insulating Solids, in: Proc. Internat. School of Phys. "Enrico Fermi", Course III, Ed. E. BURSTEIN, Academic Press, New York 1972.
[22] V. WAGNER, G. DOLLINGER, and G. LANDWEHR, Verh. DPG (VI) **10**, HL 164 (1975).
P. GROSSE, V. WAGNER, and H. BURKHARD, to be published.
[23] A. MORITANI, M. FUJIOKA, and J. NAKAI, Japan. J. appl. Phys. **15**, 1523 (1976).
[24] R. DROPE, Dissertation, Aachen 1975.

(Received August 8, 1977)